JAERI-M
7696

GRIDS HEAT LOADING OF AN ION SOURCE IN TWO-STAGE ACCELERATION SYSTEM

May 1978

Yoshikazu OKUMURA, Yoshihiro OHARA and
Tokumichi OHGA

日本原子力研究所
Japan Atomic Energy Research Institute

この報告書は、日本原子力研究所がJAERI-Mレポートとして、不定期に刊行している研究報告書です。入手、複製などのお問合わせは、日本原子力研究所技術情報部（茨城県那珂郡東海村）あて、お申しこしください。

JAERI-M reports, issued irregularly, describe the results of research works carried out in JAERI. Inquiries about the availability of reports and their reproduction should be addressed to Division of Technical Information, Japan Atomic Energy Research Institute, Tokai-mura, Naka-gun, Ibaraki-ken, Japan.

JAERI - M 7696

Grids Heat Loading of an Ion Source in Two-Stage Acceleration System

Yoshikazu OKUMURA, Yoshihiro OHARA and Tokumichi OHGA

Division of Thermonuclear Fusion Research,
Tokai Research Establishment, JAERI

(Received April 28, 1978)

Heat loading of the extraction grids, which is one of the critical problems limiting the beam pulse duration at high power level, has been investigated experimentally, with an ion source in a two-stage acceleration system of four multi-aperture grids. The loading of each grid depends largely on extraction current and grid gap pressures; it decreases with improvement of the beam optics and with decrease of the pressures. In optimum operating modes, its level is typically less than ~2% of the total beam power or ~200 W/cm^2 at beam energies of 50-70 kV.

Keywords: Ion Source, Extraction Grid, Heat Loading, Two-Stage Acceleration System, Gas Pressure, Beam Optics

JAERI－M　7696

二段加速イオン源の引き出し電極の熱負荷

日本原子力研究所東海研究所核融合研究部
奥村　義和・小原　祥裕・大智　徳道

（1978年4月28日受理）

高パワーのビームを長時間引き出す場合に大きな問題となる引き出し電極の熱負荷が，二段加速イオン源において実験的に調べられた。電極の熱負荷は，引き出し電流値と電極間の残留ガス圧に大きく依存し，ビームの発散が良い程，またガス圧が低いほど，熱負荷は小さくなる。ビームエネルギーが50～70 KVの時，最適の状態では，それは全ビームパワーの2％以下（200 W／cm^{2}以下）である。

Contents

目　　次

1. Introduction

The ion sources of the neutral beam injectors for next generation fusion experiments are required to produce ion beams of long duration at high power level. For example, the requirements for the ion sources of JT-60 injectors are to produce ion beams of 75 keV, 35 A for 2-10 sec. One of the most important problems associated with these requirements are the heat loading of the ion extraction grids. Increases in beam energy and in pulse duration time will raise the loading, which shorten the grid life time. An effective cooling method of the grids should be developed, while efforts shall be made to reduce the loading to a permissible value.

At present, most ion sources used in neutral beam injectors employ the simple accel-decel system, and in this "single-stage" acceleration system the heat loading of the grids is studied in some detail.[1),2),3),4)] But as the required beam energy increases (e.g. $\geqslant$50keV), the single-stage acceleration system becomes difficult to produce high power density beams due to the electrical breakdown problems amoung the extraction grids. For high energy accelerator sources, the "two-stage" acceleration system has been used. Compared with the single-stage system composed of accel-decel three grids, the two-stage system has an additional forth grid called "gradient grid", which reduces the breakdown problems and provides capability of electrostatic focusing. As for the heat loading of the grids, two-stage system is considered to reduce the loading by dividing it between the stages.[2)] However, experimental measurements of the grid loading of the two-stage system have not been made so far.

In this paper, we present the calorimetrically measured heat loading obtained with the two-stage system, and discuss the causes of grid loading.

2. Experimental Procedure

The experiment has been performed with a JAERI 7-cm duo-pigatron plasma source with two-stage acceleration system. (see Fig.1) The two-stage acceleration system is composed of four multi-aperture grids called plasma grid, gradient grid, suppressor grid and exit grid, respectivly. The cross section of a set of apertures in those grids and the applied voltage across the grids are shown in Fig.2. The ion extraction voltage V_{ext} is applied between the plasma and gradient grid, and the acceleration voltage V_{acc} is applied between the gradient and exit grid. The exit grid is grounded electrically. The suppressor grid is biased at negative voltage V_{dec} with respect to the exit grid to suppres electron backstream from a down stream beam plasma region. In this experiment, V_{dec} is fixed to 1.6 kV and the total acceleration voltage V_{tot} ($= V_{ext} + V_{acc}$) ranges from 50 kV to 70 kV. The extraction gap distance d_{ext} , the acceleration gap distance d_{acc} and the deceleration gap distanve d_{dec} are fixed to 6 mm, 6 mm or 4.5mm and 2.5 mm, respectively.

Each grid is made of 15 cm diam. copper disk with 83 apertures over central 5 cm diam. area. The aperture pattern is split into five sections by six water lines. (See Fig.3) The transparency of the grids is 43%. The grid thichness is 2.0 mm in the plasma and exit grids and 1.5 mm in the gradient and suppressor grids.

Hydrogen gas is supplied continuously into a hot cathode chamber. Pressures are measured always both in the hot cathde chamber and in a vacuum chamber. In usual operations, these pressures are 0.04 Torr and 2.0×10^{-4} Torr, respectively, corresponding to the gas flow of 1.2 Torr·l/sec.

Heat loading of each grid and the beam-dumner,which is 20 cm diam. and is placed 1.6 m apart from the extractor, are measured calorimetrically by the temperature difference between the inlet and outlet cooling water. The e-folding half-width beam divergence is measured by the scanning calorimeter set 1.0 m apart from the extractor. The extraction current is up to 2.0 A at 70 kV with a typical pulse length of 100msec and a duty cycle of 1/10 - 1/30.

3. Experimental Results and Discussion

3.1 Causes of grid loading

Possible causes of the grid loading are summarised in Fig.4. They are classified into three groups;

(1) direct interception of ions being accelerated (correspond to 2,3,4 in Fig.4)

(2) production of secondary particles in the grid gaps by beam-gas interactions (5,6 in Fig.4)

(3) ions accelerated toward the suppressor grid from the down-stream beam plasma region (7 in Fig.4)

In each case, energetic ions and neutrals impinging the grids release secondary electrons. These secondaries are accelerated toward the high potential region and most of them are intercepted by other grids causing heat loading.

3.2 Heat loading due to direct interception

If the pressure in the gaps and neutralizer region were low enough, the grid loading would be only due to direct interception of beam ions and resulting secondary electrons. The number of the intercepted ions may depend on the grid geometries and associated beam optics.

Fig.5 shows the calorimetrically measured heat loading of the grids and the beam dumper as a function of exracted current, where V_{ext} = 15 kV , V_{acc} = 35 kV and $d_{ext} = d_{acc}$ = 6 mm. The heat loading is normalized by extracted beam power $(V_{ext} + V_{acc}) \times I_{acc}$. The gradient grid current I_g , suppressor grid current I_{dec} and the beam divergence are also shown. The heat loading of the plasma grid is composed of loading from the source plasma and loading due to the presence of the beam. The total loading is shown by the dotted line. This figure indicates that the fraction of the grids have minimum values at I_{acc} = 0.8 A, where beam divergence is close to its minimum, and increase monotonically as I_{acc} increases or decreases from this optimum value. Since a background gas pressure is kept constant through the experiment, the increase of the grid loading on both sides of the optimum value can be attributed to interception of primary ions and secondary particles by the grids due to the

undesiably shaped ion emitting surface.

The currents flowing in the gradient grid I_g and in the suppressor grid I_{dec} should be noticed. They are expressed as

$$I_g = (1 + \bar{\gamma}_2) i_2 - C_{32}\bar{\gamma}_2 i_3$$

$$I_{dec} = (1 + \bar{\gamma}_3) i_3$$

Where i_2 and i_3 are positive ion currents into the gradient grid and the suppressor grid, respectively, $\bar{\gamma}_2$ and $\bar{\gamma}_3$ are the secondary electron emission coefficients avaraged over the incident ion energy for these grids, respectively, and C_{32} is a geometry factor, <1, which is defined by the ratio of the secondary electrons intercepted by the gradient grid to the total secondary electrons emit from the suppressor grid.

One may find that I_g is negatively small at low value of I_{acc}, and with increasing I_{acc}, I_g turns to positive and increases rapidly. From above equations, the positive I_g indicates that the direct interception by the gradient grid is dominant, while the negative I_g indicates that the secondary electron inflow from the suppressor grid is dominant. Therefore, the sharp increase of I_g toward higher I_{acc} is mainly due to direct interception by the gradient grid, which suggests that the meniscus of an ion emitter surface becomes too convex and the ion beam is divergent in the extraction gap. An increase of the direct interception by the suppressor grid toward lower I_{acc} is also envisaged from the suppressor grid current I_{dec} and the grid loading.

Such tendency is seen more evidently when the field intensity ratio f becomes small, where f is defined by the ratio of electric field intensity in the extraction gap to that in the acceleration gap, and is expressed as $f = d_{acc}V_{ext} / d_{ext}(V_{acc} + V_{dec})$. Thus f represents the lens effect of the gradient grid. When f is smaller than unity, the gradient grid forms the positive lens, and the lens effect becomes large as f becomes small. Fig.6 shows the heat loadings, grid currents and beam divergence as a function of I_{acc}, when f= 0.25 . The total acceleration voltage and grid gap distance are the same as those in Fig.5, where f=0.43.

Most characteristics in Fig.6 are similar to those in Fig.5 except for some points. Firstly, the beam divergence decreases above the optimum value of I_{acc}, where the fraction of heat loadings of the grids have minimum values, in spite of sharp increases of the gradient and plasma grid loadings. The divergence is reduced to 0.98° at I_{acc} = 0.6A. Such a small beam divergence can be explained by the following picture; although fraction of ions intercepted by the gradient grid increases above the optimum value of I_{acc}, the ions that have passed through the gradient grid are focused by the strong positive lens effect. Secondary, the heat loading of the exit grid decreases with decreasing field intensity f, as one can see from Fig.5 and Fig.6 . This is also due to the strong focusing effect, which prevents the direct interception by the exit grid. Considering that the exit grid generally receives the most loading in a single-stage acceleration system, this is one of the advantageous characteristics of the two-stage acceleration system.

3.3 Heat loading resulting from beam-gas interactions in the gaps

Depending upon the efficiency of arc dischages, some fraction of neutral gas flows out of the source plasma, and an appreciable background gas pressure is always present in the grid gaps. Some of the primary ions ionize and charge-exchange with the background gas in the gaps, and create slow ions and electrons. These slow ions are accelerated and some of them are intercepted by the grids, causing the heat loading and also producing secondary electrons. The secondary electrons are accelerated backward and cause the heat loading.

To investigate the heat loading resulting from beam-gas interactions, we varied the background gas pressure in the gaps, by regulating the hydrogen gas flow rate into the hot cathode chamber. Fig.7 shows the heat loading of the grids, beam divergence and grid currents as a function of pressure in the hot cathode chamber P_{fil} , where V_{ext} = 15 kV, V_{acc} = 35 kV, d_{ext} = d_{acc} = 6 mm and I_{acc} = 0.8 A. I_{acc} was chosen so as to minimize the fraction of heat loading of the grids in Fig. 5. The background gas pressure in the gaps is almost proportional to the filling pressure P_{fil}. As seen from this

figure, the beam divergence is scarcely influenced by the pressure in the range of P_{fil} = 0.03-0.08 Torr. Namely, the shape of beam envelop is not changed by P_{fil} and the amount of direct interception can be regarded to be almost constant in our operation range of pressure. The pressure in the beam-plasma region changes from 1.1×10^{-4} to 3.6×10^{-4} Torr, corresponding to the change of P_{fil} (0.02-0.07 Torr). As will be discussed in the following section, the amount of ion back-streaming from beam-plasma region is considerably small compared with the cold ions produced in the grid gaps within our experimental pressure range. Therefore, the increment of heat loading in Fig.7 is mainly caused by charge exchange and ionization in the grid gaps.

Since the heat loading increases almost linealy with increasing P_{fil}, the extrapolated value of the heat loading when P_{fil} approaches zero indicates the loading due to direct interception. The extrapolated values of the heat loading of the plasma and gradient grids are neary zero, while the exit grid receives a considerable loading even if the pressre approaches to zero. Therefore, we can conclude as follows; the heat loading of the exit grid is mainly due to direct interception and , when I_{acc} is optimum, that of the gradient grid is due to the impact of the secondary particles produced by beam-gas interactions.

3.4 Heat loading due to ion back-streaming from the beam-plasma region

In neutralizer cell, the primary beam ionizes the background gas, generating slow ions and electrons. Slow ions are also produced by the charge exchange of beam ions with the gas. Some of the ions that are present near the exit grid are accelerated backward and reach the suppressor grid with an energy corresponding to V_{dec} . They cause heat loading with simultaneous generation of secondary electrons. These secondary electrons in turn reaches the gradient grid, plasma grid or exit grid resulting in heat loading, either.

In the present experiment, the ion source is not followed by a neutralizer cell and the pressure in the beam-plasma region, downstream the exit grid, is low enough that the heat

loading due to ion back-streaming is negligible. However, in practical neutral beam injector the pressure in the neutralizer cell shall be 1 - 3 x 10^{-3} Torr and ion back-streaming becomes a serious source of the heat loading.

To investigate the loading due to ion back-streaming, we changed the pressure in the beam-plasma region by controlling hydrogen gas flow rate supplied directly to the vacuum chamber, while keeping a constant gas flow rate into the hot cathode chamber. Fig.8 shows the heat loading of each grid for V_{ext} = 15 kV, V_{acc} = 35 kV and I_{acc} = 0.6 A as a function of pressure in the vacuum chamber, a pressure that is nearly equal to that in the beam-plasma region. The heat loading of the gradient grid is affected significantly by the pressure P_{vac}, indicating that a greater part of the secondary electrons accelerated backward is intercepted by the gradient grid. The suppressor grid current I_{dec} increases linealy with increasing pressure P_{vac} and becomes larger than 0.1 x I_{acc} at a chamber pressure higher than 1.5 x 10^{-3} Torr.

Since the pressure in the grid gaps increases with P_{vac}, the increment of grids loading is partly due to the beam-gas interactions in the grid gaps.

3.5 Reduction of heat loading by aperture shaping

According to the design of ion source for JT-60 injector, 75 kV ion beam shall be extracted with current density of 0.27 A/cm^2 through 40% transparency extraction grids. Here, one percent dissipation of the beam power in the grid corresponds to the heat loading of 135 W/cm^2. Considering that the permissible heat loading for attaining ten second operation would be about 150 W/cm^2, we must reduce the heat loading to about one percent of the beam power at high extraction power. As seen from Figs.5 and 6, however, the heat loadings of the plasma and gradient grids increase significantly at higher extraction current and become greater than one percent because of increase of impinging ions on the gradient grid.

In order to reduce these heat loadings, we tried to enlarge the aperture diameter of the gradient grid to 4.3 mm, as shown by the Grid Type 2 in Fig.9. Next, we changed the aperture shape of the plasma grid to extract higher current density

beam. (Grid Type 3) Figs.10 and 11 show the heat loadings, beam divergence and grid currents as a function of I_{acc} in case of Grid Type 2 and 3, respectively, where operation parameters such as V_{ext}, V_{acc}, P_{fil} and P_{vac} are the same as those of Fig.6. (Grid Type 1) Comparing Figs.10 and 11 with Fig.6, we see that the heat loading of the gradient and plasma grids increase more gradually at higher extraction current by these aperture shapings. Although the aperture shape of the gradient and plasma grids has great influence on beam optics, the beam divergence is not changed for the worse.

Finally, we tried to extract 70 keV beam with grids of Type 3. Fig.12 shows the grid loading at V_{ext}= 30 kV, V_{acc}= 40 kV, d_{ext}= 6 mm and d_{acc}=4.5 mm. (f = 0.56) The loadings are only slightly affected by the extraction current I_{acc} within a limited range of measurement. The plasma grid receives the highest loading of the four, 180 W/cm^2 at I_{acc}= 2.0 A (0.25 A/cm^2), of which 50% is due to presence of the beam and 50% is from source plasma. The exit grid receives a considerable loading, 85 W/cm^2 at I_{acc}= 2.0 A, because the field intensity ratio f is large. In the present experiment, the ion source is operated with pulse duration of 100 msec. Operation with longer pulse duration will be possible on the present heat loading level.

4. Conclusion

The heat loading of the extraction grids is measured calorimetrically in the two-stage acceleration system.

In usual operation modes, the plasma gris receives the most loading of the four grids, which is composed of ~50% loading from the source plasma and ~50% loading due to the secondary electrons accelerated backward. The heat loading of the gradient grid depends greatly on the extraction current I_{acc}, and at the optimum value of I_{acc}, the loading is mainly due to the direct interception of the primary ions. That of the exit grid, which is mainly due to the direct interception, depends on beam optics and therefore depends greatly on the field intensity ratio f. The suppressir grid receives the

smallest.

The ion back-streaming from the beam plasma region is negligible when the pressure in the neutralizer cell is lower than $\sim 10^{-3}$ Torr, but it becomes a serious source of the heat loading above this pressure.

In order to reduce the grid loading, the shape of the extraction grids is modified. By this modification, we have reduced the gradient and plasma grid loading considerably at higher extraction current without changing beam optics for the worse.

Acknowledgement

The authors are grateful to S.Matsusa, H.Shirakata and other members in the plasma heating laboratory for their valuable discussions.

References

1) H.C.Cole et al., CLM-P 313 (1972)

2) L.D.Stewart et al., in Proc. of the 2nd Sympo. on Ion Sources and Formation of Ion Beams, Berkley, California, Oct. 1974

3) J.H.Fink et al., in Proc. of the 6th Sympo. on Engeneering Problems of Fusion Reserch, San Diebo, California, Nov.1975

4) S.Matsuda et al., JAERI-M6431 (1976)

Figure Captions

Fig. 1 Cross section of duopigatron ion source with two-stage acceleration system

Fig. 2 Cross section of a set of apertures of extraction grids and applied voltage

Fig. 3 Aperture pattern of the grid

Fig. 4 Possible causes of the grid loading

Fig. 5 Heat loading of each grid and beam dumper, beam divergence $\omega_{1/e}$ and grid currents I_g, I_{dec} vs. extraction current I_{acc}, where $(V_{ext} + V_{acc}) = 50$ kV and field intensity ratio $f = 0.43$

Fig. 6 Heat loading, beam divergence and grid currents vs. extraction current I_{acc}, where $(V_{ext} + V_{acc}) = 50$ kV $f = 0.25$

Fig. 7 Heat loading, beam divergence and grid currents vs. pressure in hot cathode chamber P_{fil}, where $(V_{ext} + V_{acc}) = 50$ kV $I_{acc} = 0.8$ A

Fig. 8 Heat loading, beam divergence and grid currents vs. pressure in vacuum chamber P_{vac}, where $(V_{ext} + V_{acc}) = 50$ kV $I_{acc} = 0.6$ A

Fig. 9 Types of aperture shape

Fig.10 Heat loading, beam divergence and grid currents vs. extraction current I_{acc}, where $(V_{ext} + V_{acc}) = 50$ kV $f = 0.25$ and aperture shape is Type 2

Fig.11 Heat loading, beam divergence and grid current vs. extraction current I_{acc}, where $(V_{ext} + V_{acc}) = 50$ kV $f = 0.25$ and aperture shape is Type 3

Fig.12 Heat loading, beam divergence and grid currents vs. extraction current I_{acc}, where $(V_{ext} + V_{acc}) = 70$ kV $f = 0.56$

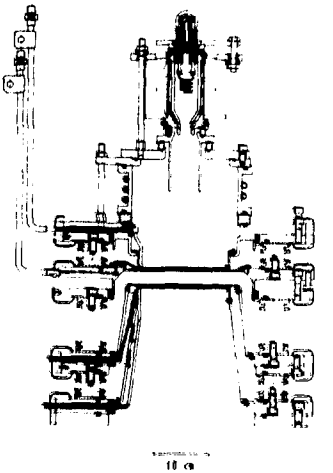

Fig. 1

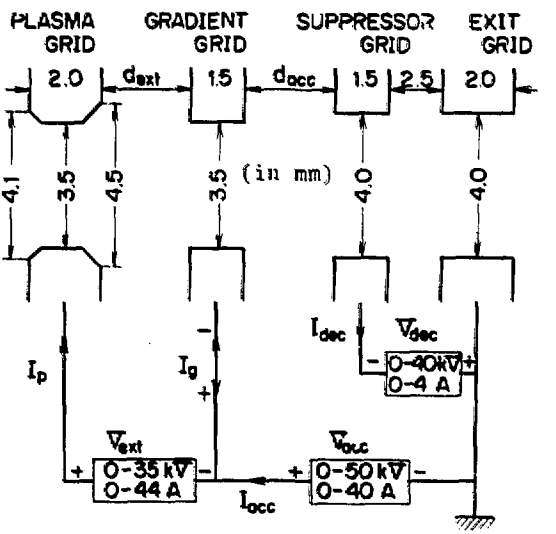
PLASMA GRID
GRADIENT GRID
SUPPRESSOR GRID
EXIT GRID
2.0
d_{ext}
1.5
d_{acc}
1.5
2.5
2.0
4.1
3.5
4.5
3.5
(in mm)
4.0
4.0
I_p
I_g
I_{dec}
V_{dec}
0-40kV
0-4 A
V_{ext}
0-35 kV
0-44 A
V_{acc}
0-50 kV
0-40 A
I_{acc}

Fig. 2

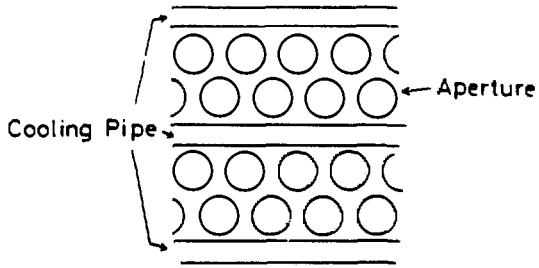
Aperture
Cooling Pipe
5 mm

Fig. 3

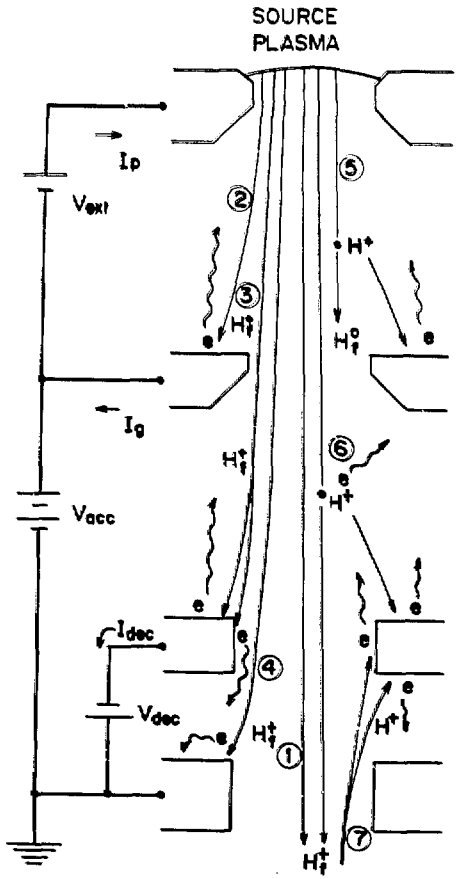
SOURCE
PLASMA
Ip
Vext
Ig
Vacc
Idec
Vdec
H+
e
1
2
3
4
5
6
7

Fig. 4

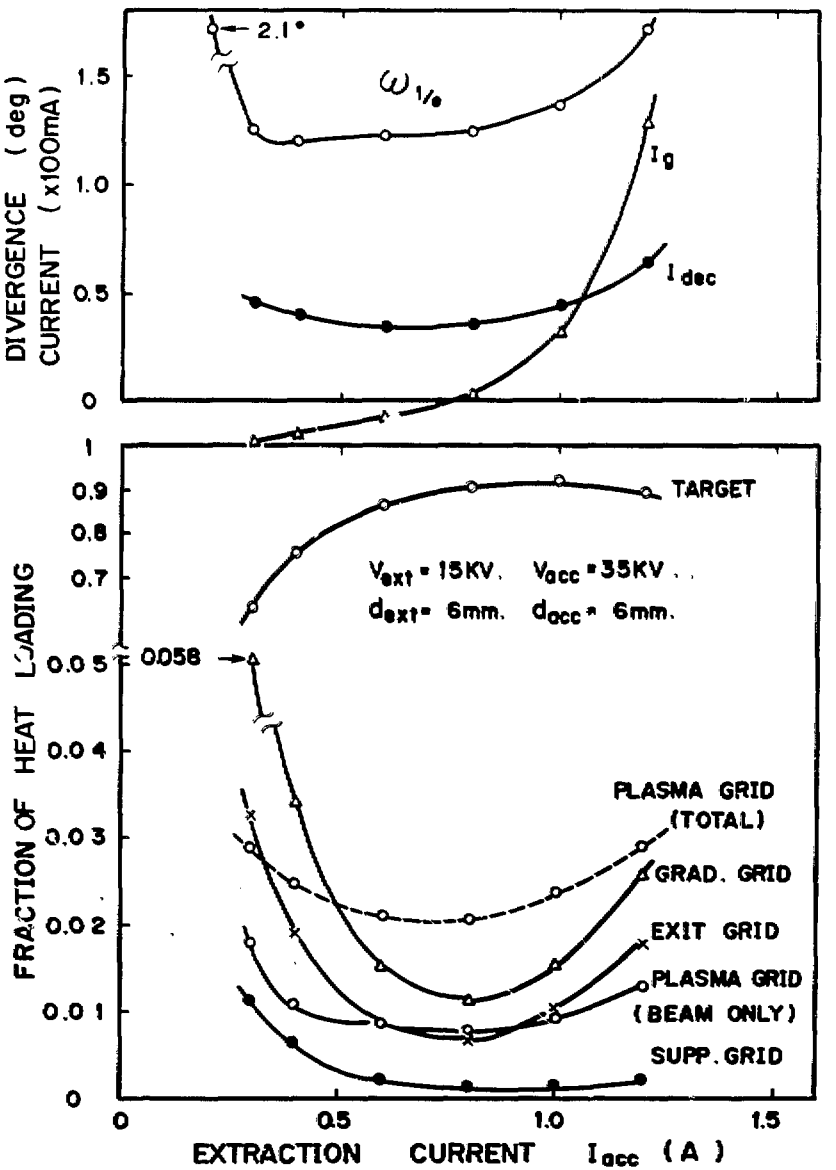
2.1°
$\omega_{1/e}$
I_g
I_{dec}
DIVERGENCE (deg)
CURRENT (x100mA)
1.5
1.0
0.5
0
TARGET
V_{ext} = 15KV, V_{acc} = 35KV
d_{ext} = 6mm, d_{acc} = 6mm
0.058
PLASMA GRID (TOTAL)
GRAD. GRID
EXIT GRID
PLASMA GRID (BEAM ONLY)
SUPP. GRID
FRACTION OF HEAT LOADING
1
0.9
0.8
0.7
0.05
0.04
0.03
0.02
0.01
0
0
0.5
1.0
1.5
EXTRACTION CURRENT I_{acc} (A)

Fig. 5

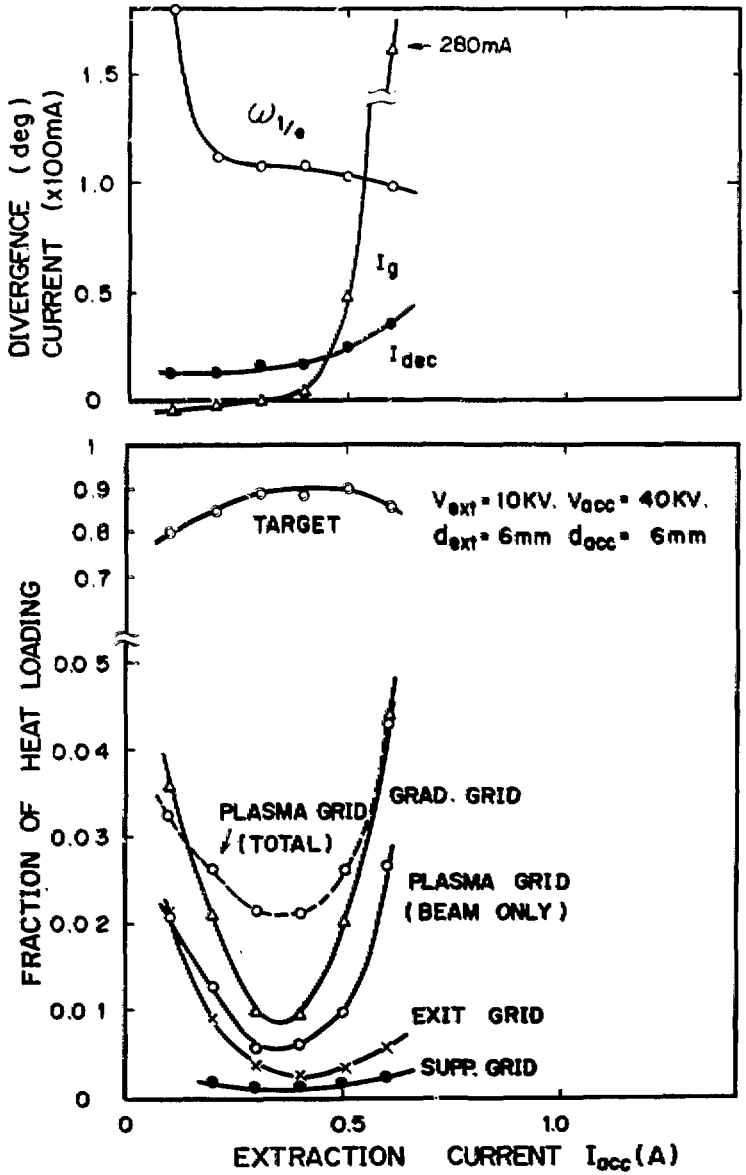
DIVERGENCE (deg)
CURRENT (x100mA)
280mA
$\omega_{1/e}$
I_g
I_{dec}
1.5
1.0
0.5
0
FRACTION OF HEAT LOADING
TARGET
V_{ext} = 10KV, V_{acc} = 40KV,
d_{ext} = 6mm d_{acc} = 6mm
PLASMA GRID (TOTAL)
GRAD. GRID
PLASMA GRID (BEAM ONLY)
EXIT GRID
SUPP. GRID
0.9
0.8
0.7
0.05
0.04
0.03
0.02
0.01
0
0.5
1.0
EXTRACTION CURRENT I_{acc}(A)

Fig. 6

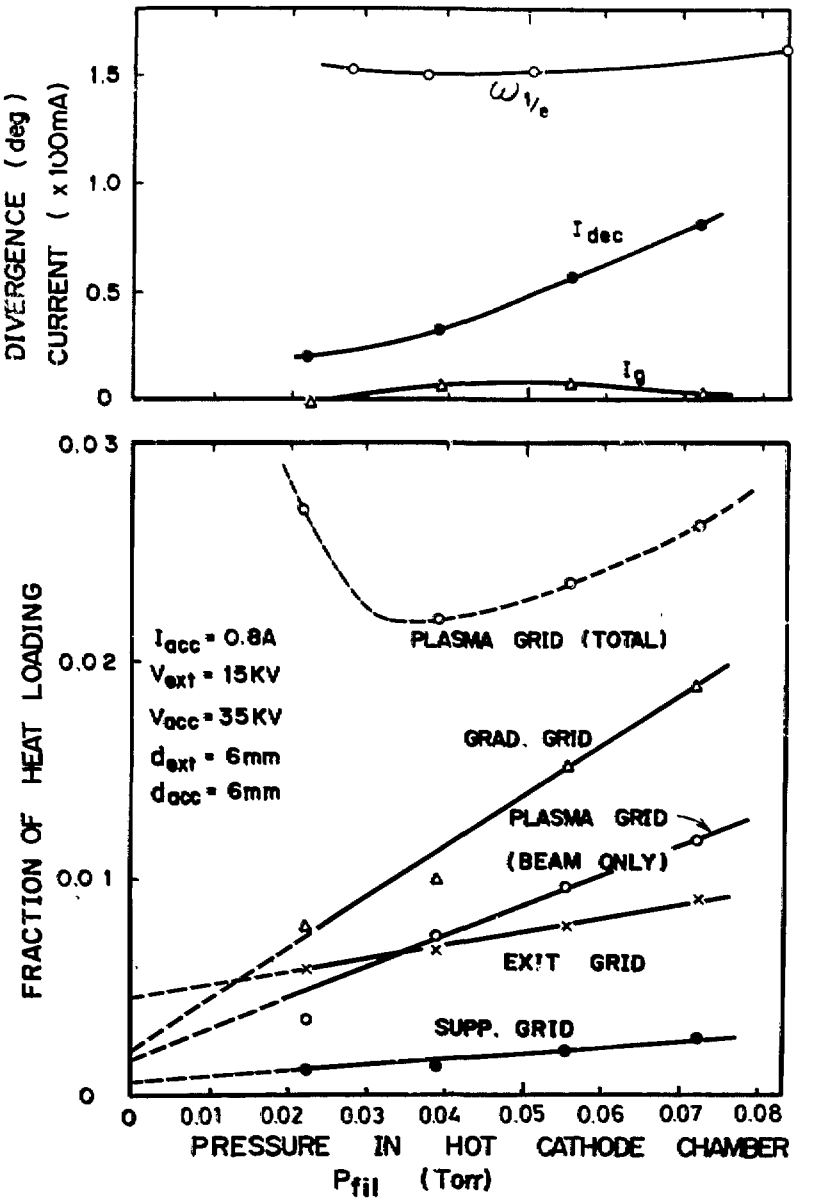
DIVERGENCE (deg)
CURRENT (x 100mA)
1.5
1.0
0.5
0
$\omega_{1/e}$
I_{dec}
I_g
FRACTION OF HEAT LOADING
0.03
0.02
0.01
0
I_{acc} = 0.8A
V_{ext} = 15KV
V_{acc} = 35KV
d_{ext} = 6mm
d_{acc} = 6mm
PLASMA GRID (TOTAL)
GRAD. GRID
PLASMA GRID
(BEAM ONLY)
EXIT GRID
SUPP. GRID
0
0.01
0.02
0.03
0.04
0.05
0.06
0.07
0.08
PRESSURE IN HOT CATHODE CHAMBER
P_{fil} (Torr)

Fig. 7

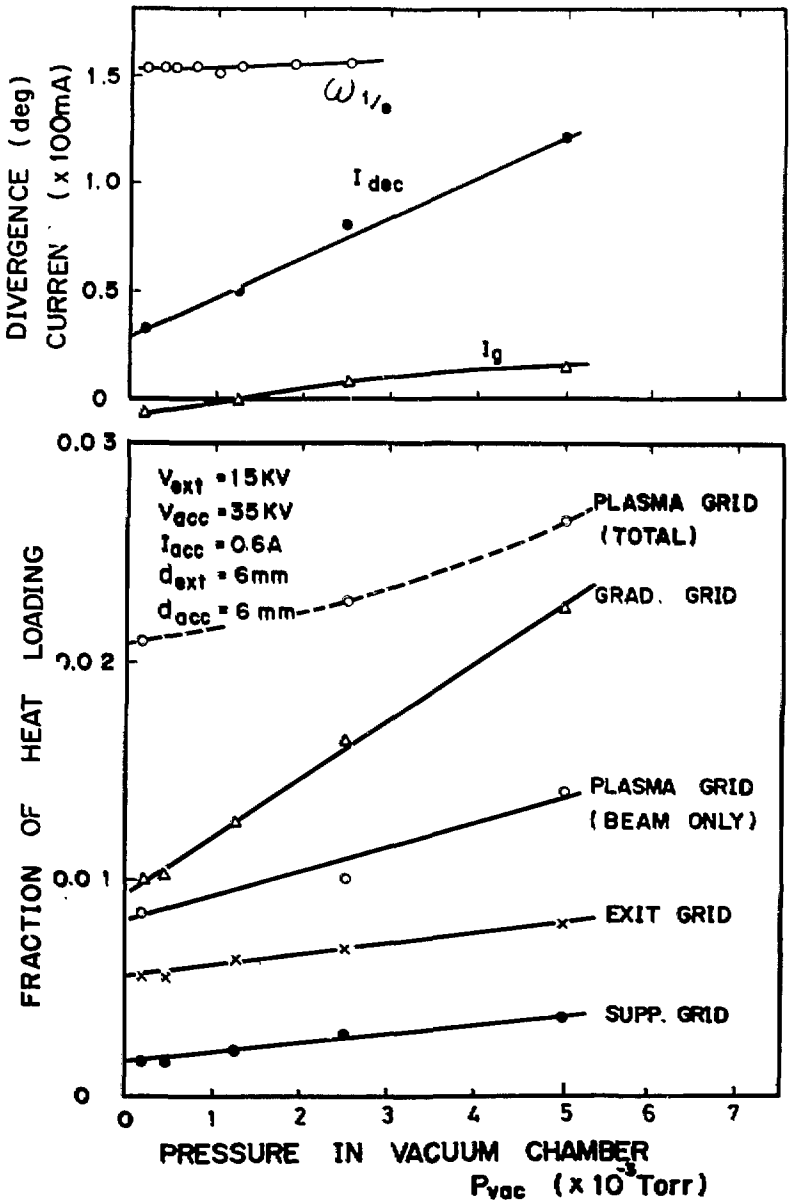
DIVERGENCE (deg)
CURREN (x100mA)
1.5
1.0
0.5
0
$\omega_{1/e}$
I_{dec}
I_g
0.03
0.02
0.01
0
FRACTION OF HEAT LOADING
V_{ext} = 15KV
V_{acc} = 35KV
I_{acc} = 0.6A
d_{ext} = 6mm
d_{acc} = 6 mm
PLASMA GRID (TOTAL)
GRAD. GRID
PLASMA GRID (BEAM ONLY)
EXIT GRID
SUPP. GRID
0
1
2
3
4
5
6
7
PRESSURE IN VACUUM CHAMBER
P_{vac} (x 10^{-3} Torr)

Fig. 8

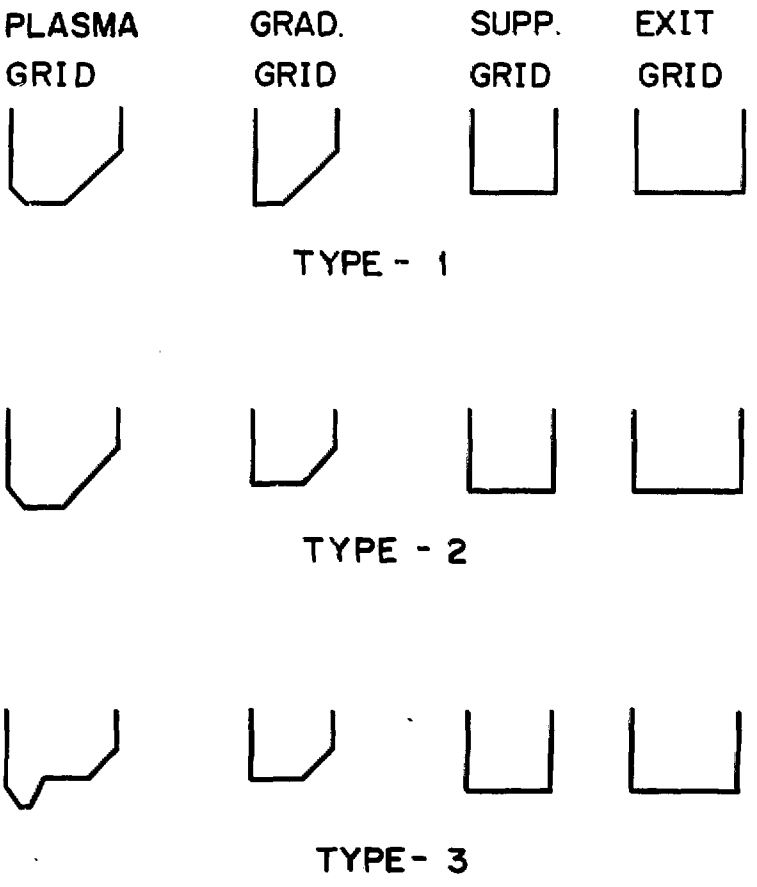

TYPES OF APERTURE SHAPE

Fig. 9

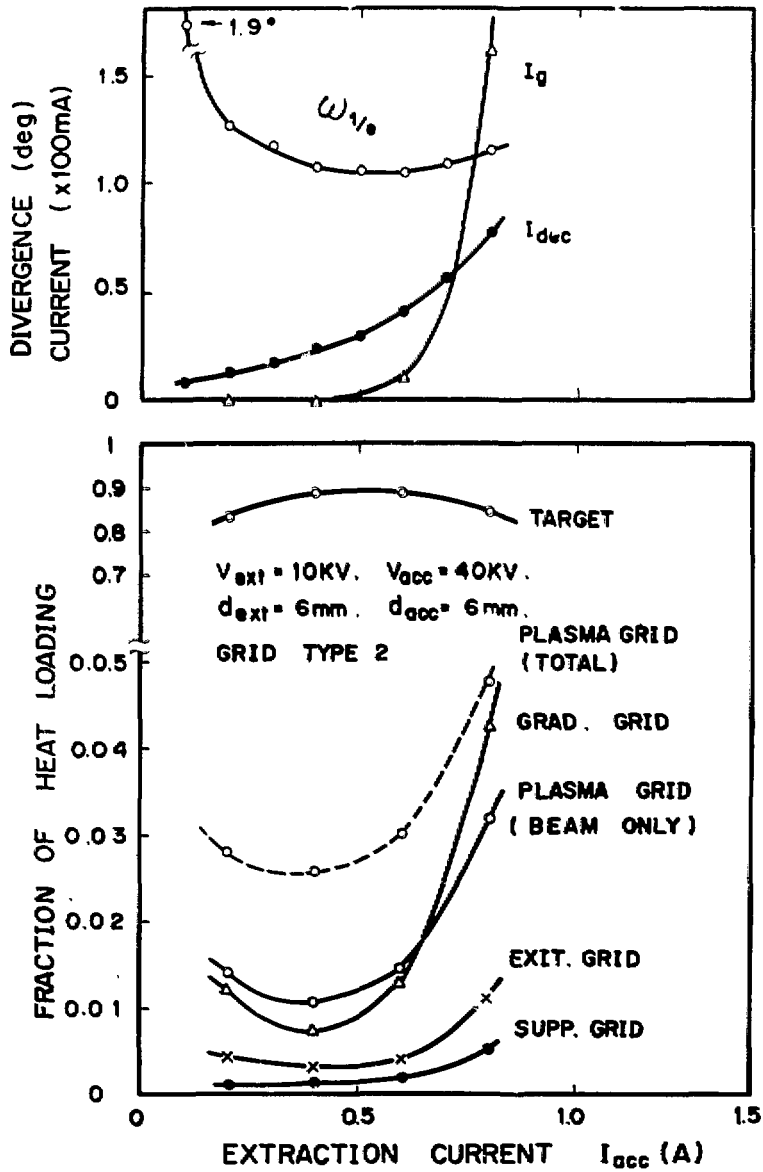
DIVERGENCE (deg)
CURRENT (x100mA)
1.9°
$\omega_{1/e}$
I_g
I_{dec}
1.5
1.0
0.5
0
FRACTION OF HEAT LOADING
TARGET
V_{ext} = 10KV, V_{acc} = 40KV,
d_{ext} = 6mm, d_{acc} = 6mm,
GRID TYPE 2
PLASMA GRID (TOTAL)
GRAD. GRID
PLASMA GRID (BEAM ONLY)
EXIT. GRID
SUPP. GRID
1
0.9
0.8
0.7
0.5
0.04
0.03
0.02
0.01
0
0
0.5
1.0
1.5
EXTRACTION CURRENT I_{acc} (A)

Fig. 10

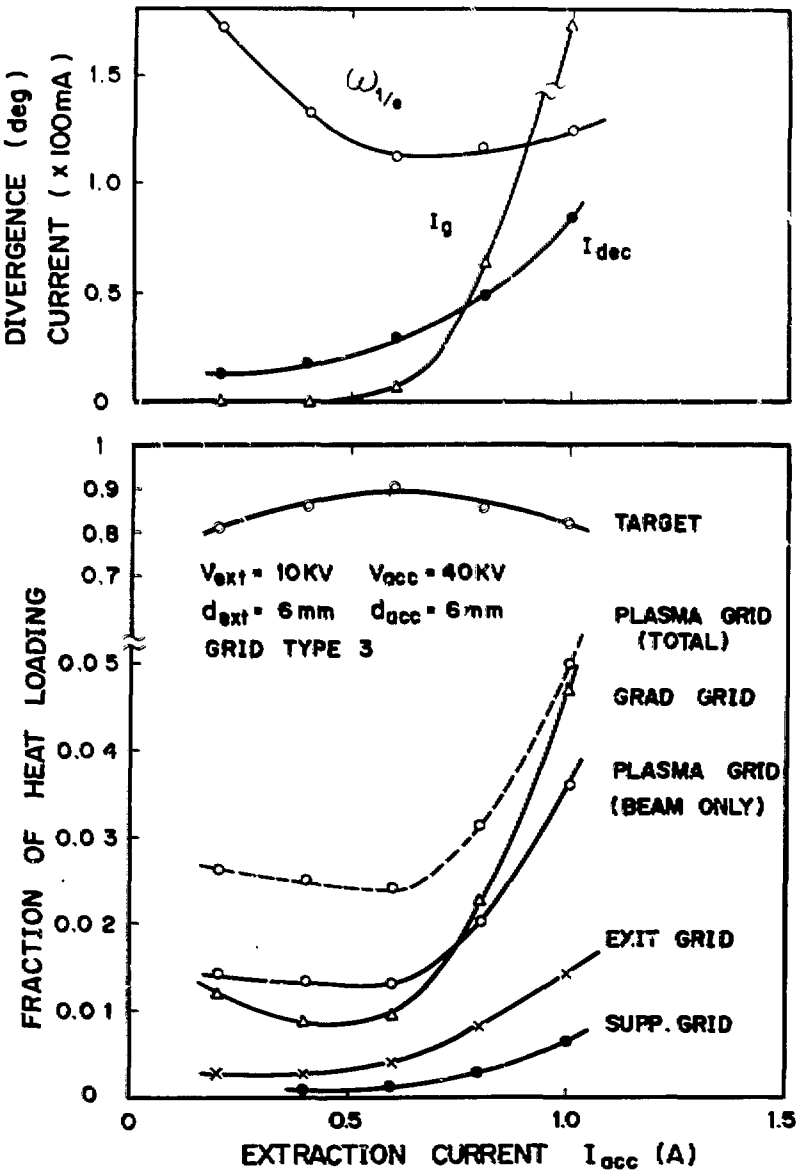
DIVERGENCE (deg)
CURRENT (x 100mA)
1.5
1.0
0.5
0
$\omega_{1/e}$
I_g
I_{dec}
FRACTION OF HEAT LOADING
1
0.9
0.8
0.7
0.05
0.04
0.03
0.02
0.01
0
TARGET
V_{ext} = 10KV V_{acc} = 40KV
d_{ext} = 6mm d_{acc} = 6mm
GRID TYPE 3
PLASMA GRID (TOTAL)
GRAD GRID
PLASMA GRID (BEAM ONLY)
EXIT GRID
SUPP. GRID
0
0.5
1.0
1.5
EXTRACTION CURRENT I_{acc} (A)

Fig. 11

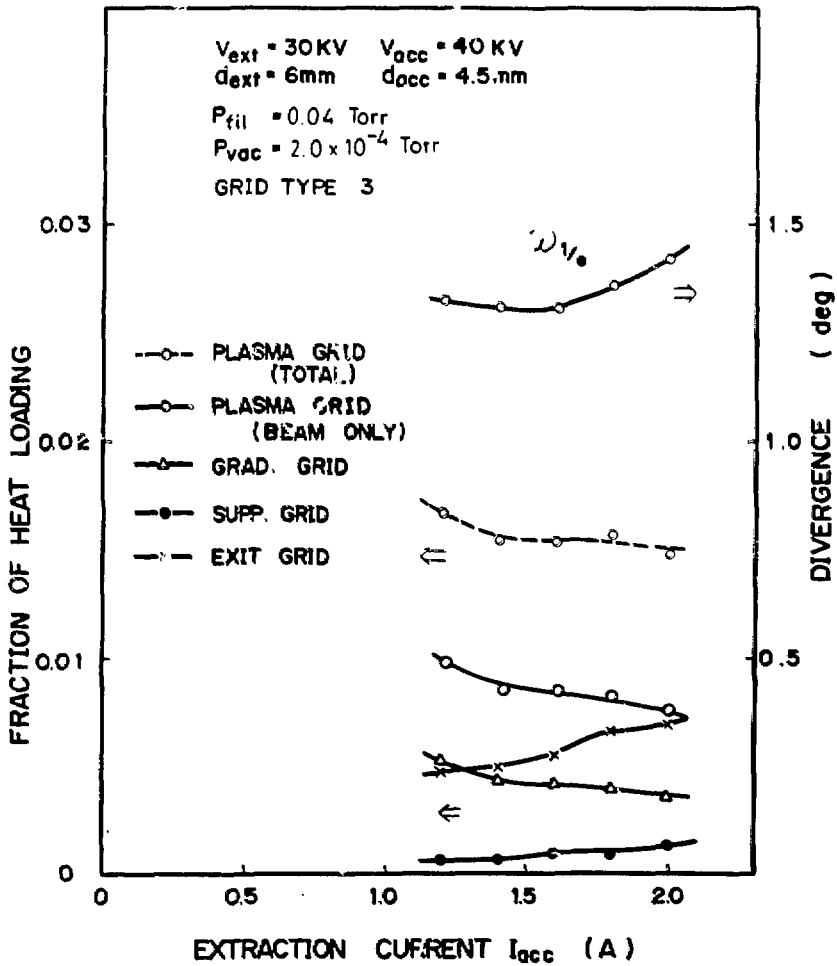
V_{ext} = 30KV V_{acc} = 40 KV
d_{ext} = 6mm d_{acc} = 4.5mm
P_{fil} = 0.04 Torr
P_{vac} = 2.0 x 10^{-4} Torr
GRID TYPE 3
PLASMA GRID (TOTAL)
PLASMA GRID (BEAM ONLY)
GRAD. GRID
SUPP. GRID
EXIT GRID
$\omega_{1/e}$
FRACTION OF HEAT LOADING
DIVERGENCE (deg)
0.03
0.02
0.01
0
1.5
1.0
0.5
0
0.5
1.0
1.5
2.0
EXTRACTION CURRENT I_{acc} (A)

Fig. 12